Defect-Selective Charge-Density-Wave Condensation in 2H-NbSe$_2$

Eunseok Oh⬤, Gyeongcheol Gye, and Han Woong Yeom⬤[*]

Center for Artificial Low Dimensional Electronic Systems, Institute for Basic Science (IBS), Pohang 37673, Republic of Korea
and Department of Physics, Pohang University of Science and Technology (POSTECH), Pohang 37673, Republic of Korea

Defects have been known to substantially affect quantum states of materials including charge density wave (CDW). However, the microscopic mechanism of the influence of defects is often elusive due partly to the lack of atomic scale characterization of defects themselves. We investigate native defects of a prototypical CDW material 2H-NbSe$_2$ and their microscopic interaction with CDW. Three prevailing types of atomic scale defects are classified by scanning tunneling microscope, and their atomic structures are identified by density functional theory calculations as Se vacancies and Nb intercalants. Above the transition temperature, two distinct CDW structures are found to be induced selectively by different types of defects. This intriguing phenomenon is explained by competing CDW ground states and local lattice strain fields induced by defects, providing a clear microscopic mechanism of the defect-CDW interaction.

Local defects possess substantial impacts on a wide range of global properties of solid materials such as mechanical, chemical, electric, and magnetic properties [1]. Impacts of defects are expected to become even more profound for many-body quantum states in low-dimensional electronic systems, including superconductivity [2,3] and charge/spin density waves [4]. In case of charge density wave (CDW), where electrons and holes at the Fermi level couple through the lattice vibration [4], charges and local lattice distortions from defects can naturally and actively intertwine with CDW [5,6]. This straightforwardly indicates that detailed microscopic structures of individual defects are crucial to understand the defect-CDW interaction. Considering that CDW is entangled intriguingly with unconventional superconductivity [7–15], understanding such an interaction has a wider implication beyond conventional CDW physics.

In spite of long-standing interests and efforts on the defect-CDW interaction, the microscopic understanding of the interaction has been limited [4]. Previous studies showed that long range CDW orders could be suppressed by impurities [16,17] or dislocated by native defects [18–20]. In addition, it was reported that CDW can locally be condensed above the transition temperature (T_c) by single native defect [21–23] or the cooperation of multiple impurities [24,25]. Most of these studies are phenomenological and microscopic mechanisms of the observed defect-CDW interactions were not clearly addressed. The limitation of the previous studies comes largely from the lack of the atomic scale characterization of the defects involved.

This situation provides us a strong motivation to reinvestigate the defect issue in a model CDW system of 2H-NbSe$_2$, where the perturbation and early condensation

of CDW around native defects or impurities were noticed previously [16,19,21]. 2H-NbSe$_2$ undergoes a phase transition at $T_c = 33$ K into a 3×3 CDW phase [26,27], which is commonly observed for the $2H$ prototype of metallic transition metal dichalcogenides (TMDCs). Like many other TMDC materials, the CDW phase in 2H-NbSe$_2$ is understood to be driven by strong momentum-dependent electron-phonon coupling without substantial Peierls-type Fermi surface instability [28]. As mentioned above, this suggests that structural degrees of freedom of defects and, therefore, detailed atomic structures of them would play important roles. However, so far, the atomic and chemical structure of the native defects have not been clarified. Adding extra complexity to this issue, the CDW ground state of 2H-NbSe$_2$ has been known for decades to be intriguingly incommensurate [29–31]. The puzzle was solved by a very recent work, which revealed the microscopic structure and mechanism of the incommensuration as due to the discommensuration network between two competing commensurate CDW structures [32]. This finding provides a better chance to understand an in-depth microscopic mechanism of the defect-CDW interaction.

In this Letter, characteristic point defect structures and their influence on the CDW of 2H-NbSe$_2$ are analyzed in detail by scanning tunneling microscopy (STM). *Ab initio* density functional theory (DFT) calculations reveal the atomic structures of three major types of defects through STM image simulations as Se vacancies (type A) on the topmost layer and Nb intercalants in the van der Waals gap at two different lateral positions (types B and C). Slightly above T_c, A/B and C type defects are found to induce selectively two different CDW structures of the pristine ground state. DFT calculations explain its origin as due to distinct local strain fields induced by defects. This work

clarifies a structural mechanism of the defect-CDW inter-action and suggests a possibility to control degenerate many-body quantum states involving CDW.

$2H$-NbSe$_2$ single crystals were grown by chemical vapor transport and cleaved at 145 K in high vacuum and transferred directly to a ultrahigh-vacuum chamber equipped with a commercial low-temperature STM. Pt/Ir tips are used for STM measurements in constant current mode at temperatures 4.3 and 40 K. We perform DFT calculations using Vienna *ab initio* simulation package [33] with the projector augmented wave method [34,35]. The Perdew-Burke-Ernzerhof exchange correlation functional [36] is used with the DFT-D2 van der Waals correction [37]. $2H$-NbSe$_2$ is modeled by a 9×9 unit cell single or double layer slabs separated by a 15 Å vacuum layer with the CDW distortion allowed. A $(4 \times 4 \times 1)$ k-point mesh and a plane wave cutoff energy of 366.5 eV are used with all atoms relaxed. STM images are simulated by the Tersoff-Hamann approximation [38] using local density of states at about 3 Å above top atoms.

The STM topography taken in Fig. 1(a) shows clearly the 3×3 CDW phase on the surface of $2H$-NbSe$_2$ at 4.3 K, well below the CDW T_c. The CDW long range order is partly broken by the extraordinary coexistence of two different CDW structures, the hollow-centered (HC) and the anion-centered (AC) CDW [Figs. 1(d) and 1(e), respectively] [32]. These structures are zoomed in Figs. 1(b) and 1(c) and clearly distinguished by their distinct STM topographies. In addition to the coexisting CDW structures, several types of native point defects appear as characteristic and strong local topographic modulations. These images are consistent with the previous STM works while the atomic scale structures were not detailed previously [19,21,39]. We identify many types of point defects [Fig. 1(a) and see Fig. S1 in the Supplemental Material [40]] whose total density is about 0.5% of all sites. In particular, three of them, denoted as A, B, and C, occupy the major population (80% of the total), and the most popular one C explains almost half of the whole population.

Topographic features of three popular defects are zoomed in Fig. 2. Defect A presents a dark hole feature, which has a deep depression at the central Se site with three bright protrusions at next-nearest Se atoms. In stark contrast, defects B and C are represented by clusters of protrusions, one brightest protrusion with nine less bright protrusions in the nearest neighbor (B) and a trimer protrusion (C). The topographic depressions or protrusions have overall consistency in both filled and empty states for a wide bias range of ± 0.5 eV [Fig. 1(a) and see Fig. S1 in the Supplemental Material [40]]. This indicates that their origins are not due to subtle electronic effects but mostly to structural distortions.

In order to clarify atomic structures underlying these characteristic topographies, we build various structure
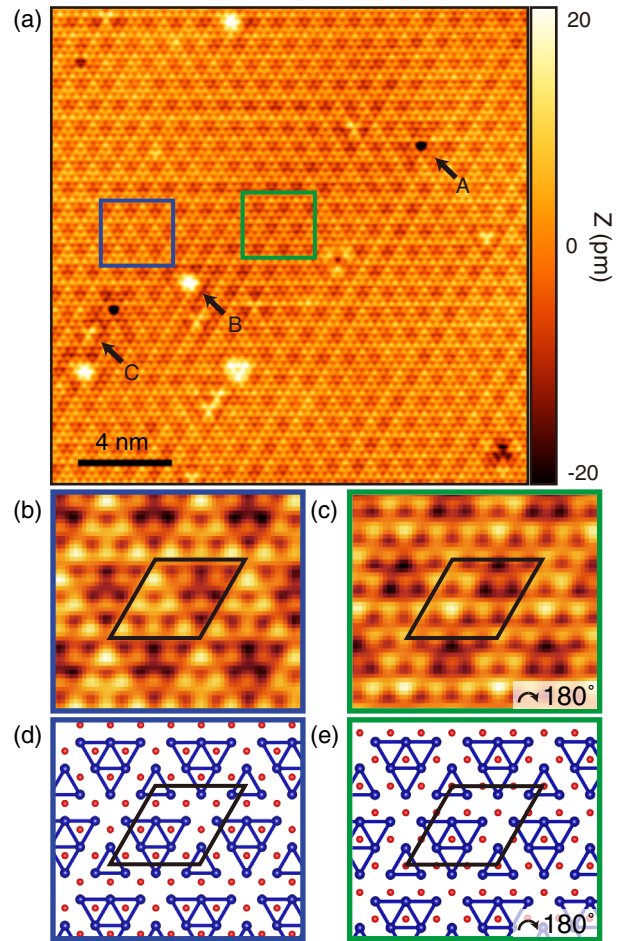

FIG. 1. Empty state STM topographic images of $2H$-NbSe$_2$ at 4.3 K. (a) Large area topographic image (bias -100 mV, tunneling current 1 nA) with major types of defects (A, B, and C) denoted. Zoomed-in images for two different CDW structures coexisting. (b) Hollow-centered (HC) CDW [blue squared area in (a)] and (c) anion-centered (AC) CDW [180° rotated image of green square area in (a)]. (d),(e) Schematic models for HC and AC CDW. 3×3 CDW unit cells are indicated.

models within DFT calculations and compare their ener-getics and their simulated STM images with experiments for a wide bias range [Fig. 1(a) and see Fig. S1 in the Supplemental Material [40]]. DFT calculations for inter-stitial defects are considered in double layer models, while the other cases are treated in single layer models. We consider Se or Nb vacancies, extra Se, Nb atoms, iodine, and oxygen atoms as adsorbates in the top layer, substitu-tionals and interstitials in the van der Waals gap. Iodine (used as the transporting agent) and oxygen (from atmos-phere) are known as the most popular impurity atoms. For the case of defect A, the deep depression [Fig. 1(a)] at the Se site straightforwardly indicates a Se vacancy on the top layer (Fig. 2 left) [21,39,41] and the corresponding DFT-simulated images agree convincingly well with the experi-ments (Fig. 2 top row and see Fig. S2 in the Supplemental
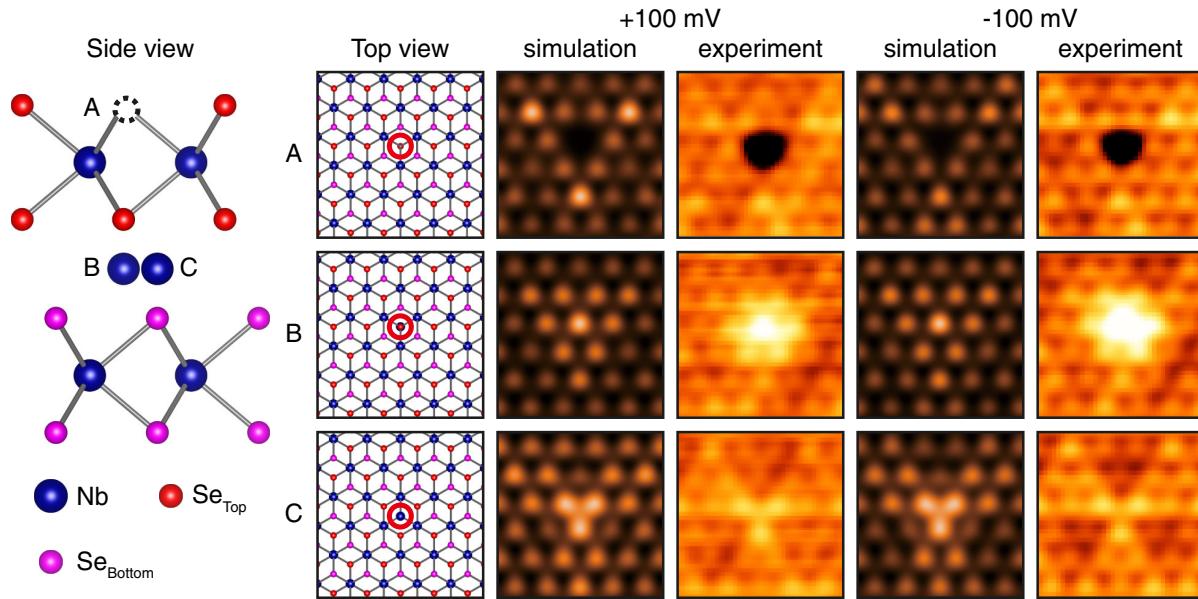
FIG. 2.   Schematic models (side and top views), STM images (+100 and −100 mV bias), and corresponding DFT simulations of defect type A (an Se vacancy in the top layer, top row), B (an Nb intercalant below a top layer Se atom, center row), and C (an Nb intercalant below the hollow site of the top layer, bottom row).

Material [40]). On the contrary, the protrusions in defects B and C [Fig. 1(a)] may correspond to adsorbed atoms on the top layer. However, the corresponding protrusions are only several tens of pm, order of magnitude smaller than expected for an adsorbate. Moreover, various trial structures with different adsorbate atoms are not successful in reproducing the experimental images. We then try many different substitutional or interstitial addition of Nb, Se, I and O. From the symmetry of the protrusions, defect B (C) can be thought to represent such atoms in the Se (hollow) site. The only successful models are Nb atoms intercalated within the van der Waals gap (Fig. 2 center and bottom row, and see Fig. S2 in the Supplemental Material [40]). Other interstitial cases of Se, I, and O can be ruled out by the mismatches in the simulated STM images (see Figs. S3 and S4 in the Supplemental Material [40]). An Nb atom on the Se (hollow) site in the van der Waals gap push atoms above them upward, which can explain the topographic protrusions of defects B and C. An anion vacancy and a cation intercalant were recently identified with very similar STM images in another rigorously studied CDW system of $1T$-TiSe$_2$ [42]. This provides extra support of the present structure models. Additionally, the tentative models for minor defects are also suggested (see Fig. S5 in the Supplemental Material [40]).

These defects, while not classified into different types, were reported to pin the phase of CDW below T_c [19] and the amplitude of CDW above T_c [21]. We focus on the effect on the CDW amplitude. A large area STM topography taken at 40 K [Fig. 3(a)] shows a number of point defects in mainly three different types. Short range CDW modulations are observed near most of defects at this high

temperature (1.21 T_c). The average length scale of these modulations around defects is about 2.75 nm extending to about eight pristine unit cells. The zoomed-in images around defect types A, B, and C [Figs. 3(b)–3(g) and see Fig. S6 in the Supplemental Material [40] for their detailed line profiles] and their Fourier transformations [Fig. 3(h)] reveal that the local CDW modulation depends unexpectedly on the defect type. That is, A/B and C defects preferentially induce the AC and HC CDW structures, respectively, which are represented by one and three bright protrusions within a single CDW unit cell, respectively. We check a large number of defects at this temperature to find very little exception in this preference [Fig. 3(a)]. The modulation around defect B has a shorter range than those around defects A and C.

In order to understand the origin of defect-selective CDW modulations, the relaxed atomic structures around each type of defects are scrutinized by DFT calculations. The calculated relaxation patterns [Figs. 4(a) and 4(b)], especially those of the Nb layer, immediately tell that defects A and C induce different structural distortions, which are largely consistent with the AC and HC CDW distortions of the pristine layer. Note the formation of Nb trimers/hexamers centered by Se atoms (hollow sites) in the topmost layer for the AC (HC) structures (colored in Fig. 4). As shown in the difference of the lattice distortions between the defect-induced and pristine CDW structures [Figs. 4(a) and 4(b) and see Fig. S7 in the Supplemental Material [40]], the strain field propagating out from defect A (C) matches reasonably with the pristine AC (HC) CDW distortions except for the strong local distortions on the nearest-neighbor atoms [Figs. 4(c) and 4(d)].
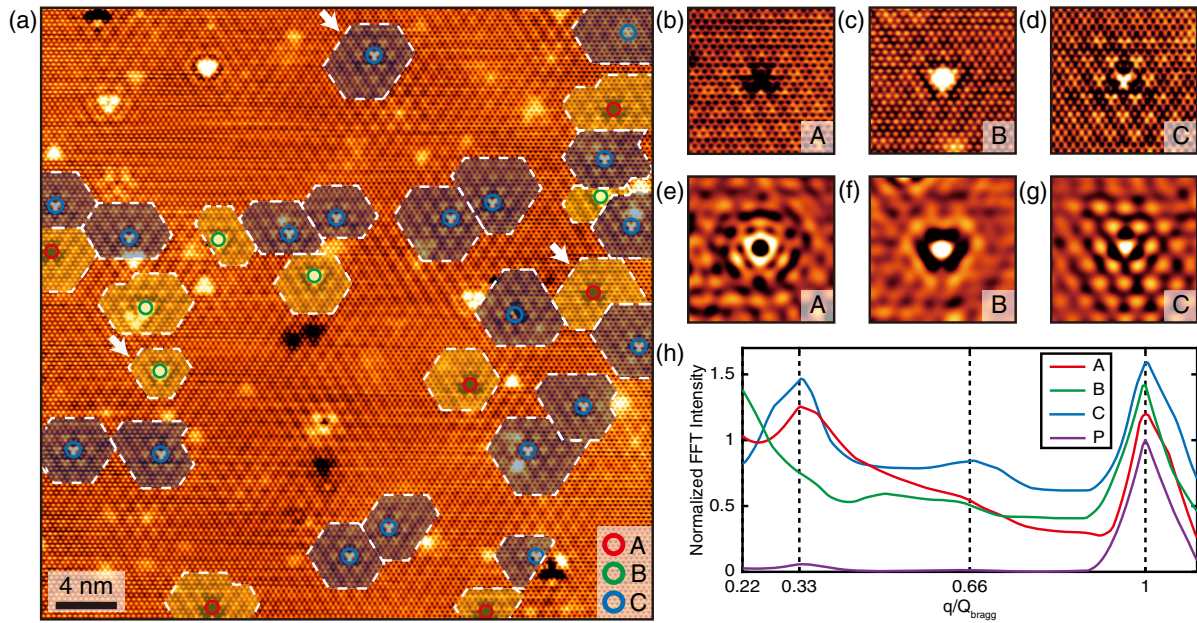
FIG. 3. (a) Large area STM topographic image of 2H-NbSe$_2$ at 40 K (bias +100 mV, tunneling current 1 nA). Local CDW modulation areas around defects A, B, and C are encircled by white dashed lines. Yellow and blue colored area within dashed lines indicate different, AC and HC, respectively, CDW structures. (b)–(d) Zoomed-in (6.15×6.15 nm^2) images around defect A, B, and C indicated by white arrows in (a). (e)–(g) Fast-Fourier-transformation filtered topographic images for (b)–(d) to enhance the CDW modulations by eliminating pristine lattice structure ($1Q/2 \leq q \leq 3Q/2$, $Q = Q_{Bragg}/3$). (h) Line profiles along the atomic wave vector in the two-dimensional FFT of zoomed-in images of (b)–(d) for defects A, B, and C. A similar line profile for a pristine area (P) is given for comparison. Offsets are given for clarity. The FFT intensity is normalized by the peak intensity at Q_{Bragg}

This characteristic difference can intuitively be understood from the local registry of defects; defect A is sitting on Se sites, but defect C is on hollow sites favoring AC or HC structures, respectively. Therefore, the extraordinary relationship between the defects and CDW can be straightforwardly understood from the structural effect, the local strain fields induced by the defects and the symmetry of the defect sites. A consistent result is obtained for defect B (see Fig. S8 in the Supplemental Material [40]). The local registry of a defect site plays a more direct role compared to the chemical identity of the defect. This seems consistent with the strong electron-lattice coupling mechanism of CDW in 2H-NbSe$_2$. At this point, we note that the major defects observed presently are not charged as they do not shift the local density of states noticeably (see Fig. S9 in the Supplemental Material [40]). This excludes the possibility of a strong electronic effect of defects. For interstitial cases (defects B and C), the above calculations were performed with simpler single layer models where an Nb intercalant is attached at the bottom layer at a distance optimized in the double layer models. The double layer models have the uncertainty in the CDW stacking between layers which affects the distortion patterns subtly around a defect. However, the overall conclusion does not depend significantly on the choice models (see Figs. S10 and S11 in the Supplemental Material [40]).
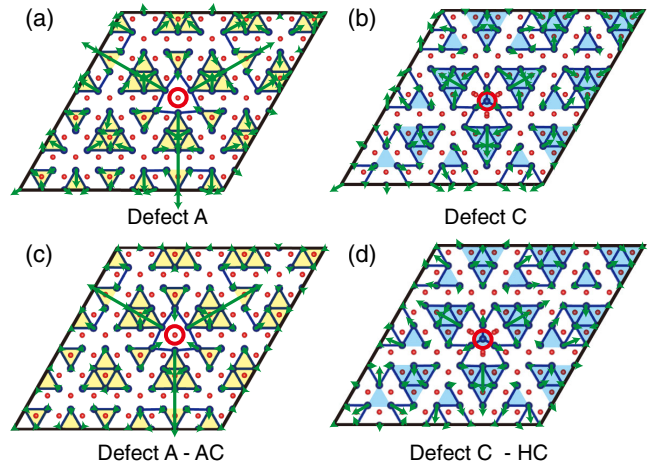

FIG. 4. (a),(b) DFT-simulated atomic structures around defects A and C. Solid lines represent contracted Nb——Nb bonds (< 3.475 Å). Yellow (blue) colored areas indicate to Nb trimers/hexamers of AC (HC) CDW structures without defects. Green arrows indicate the displacements (enlarged by 50 times) at each Nb atom from the pristine structure. Red circles indicate defect positions. (c),(d) The same DFT-simulated atomic structures where the green arrows indicate the difference of the Nb distortions from the AC (c) or HC (d) CDW structures.

Very interestingly, the preferential coupling of the different CDW structures with different types of defects is not noticeably for the fully developed CDW phase at 4.3 K [Fig. 1(a) and see Fig. S12 in the Supplemental Material [40]]. There is no noticeable difference of the populations of A/B and C defects in AC and HC CDW domains and no apparent CDW pinning effect is observed. While a conclusive statement is premature, we suggest that the extra energy gain of the unusual topological network formation of the HC and AC CDW domains [32,43] prevails the CDW pinning energy by defects [19]. The other aspect not considered here is the interlayer locking of CDW, which would provide extra energy gain over the defect pinning. In any case, the selective local condensation of CDW can be explained by the distinct local strain fields of the defects, which is in turn consistent with the strong electron-lattice coupling mechanism of CDW. This work provides a clear microscopic mechanism of the CDW-defect interaction and suggests a route to control competing many-body quantum states by defects.

---

*yeom@postech.ac.kr

[1] R. J. Tilley, *Defects in Solids* (John Wiley Sons, Inc., Hoboken, New Jersey, 2008).

[2] A. V. Balatsky, I. Vekhter, and J.-X. Zhu, Rev. Mod. Phys. **78**, 373 (2006).

[3] H. Alloul, J. Bobroff, M. Gabay, and P. J. Hirschfeld, Rev. Mod. Phys. **81**, 45 (2009).

[4] G. Grüner, Rev. Mod. Phys. **60**, 1129 (1988).

[5] X.-L. Wu, P. Zhou, and C. M. Lieber, Phys. Rev. Lett. **61**, 2604 (1988).

[6] X. L. Wu and C. M. Lieber, Phys. Rev. B **41**, 1239 (1990).

[7] A. J. Achkar, R. Sutarto, X. Mao, F. He, A. Frano, S. Blanco-Canosa, M. Le Tacon, G. Ghiringhelli, L. Braicovich, M. Minola, M. Moretti Sala, C. Mazzoli, R. Liang, D. A. Bonn, W. N. Hardy, B. Keimer, G. A. Sawatzky, and D. G. Hawthorn, Phys. Rev. Lett. **109**, 167001 (2012).

[8] G. Ghiringhelli, M. Le Tacon, M. Minola, S. Blanco-Canosa, C. Mazzoli, N. B. Brookes, G. M. De Luca, A. Frano, D. G. Hawthorn, F. He, T. Loew, M. M. Sala, D. C. Peets, M. Salluzzo, E. Schierle, R. Sutarto, G. A. Sawatzky, E. Weschke, B. Keimer, and L. Braicovich, Science **337**, 821 (2012).

[9] J. Chang, E. Blackburn, A. T. Holmes, N. B. Christensen, J. Larsen, J. Mesot, R. Liang, D. A. Bonn, W. N. Hardy, A. Watenphul, M. v. Zimmermann, E. M. Forgan, and S. M. Hayden, Nat. Phys. **8**, 871 (2012).

[10] T. Wu, H. Mayaffre, S. Krämer, M. Horvatic, C. Berthier, W. N. Hardy, R. Liang, D. A. Bonn, and M.-H. Julien, Nature (London) **477**, 191 (2011).

[11] J. M. Tranquada, B. J. Sternlieb, J. D. Axe, Y. Nakamura, and S. Uchida, Nature (London) **375**, 561 (1995).

[12] H.-H. Wu, M. Buchholz, C. Trabant, C. F. Chang, A. C. Komarek, F. Heigl, M. v. Zimmermann, M. Cwik, F. Nakamura, M. Braden, and C. Schüßler-Langeheine, Nat. Commun. **3**, 1023 (2012).

[13] K. Fujita, A. R. Schmidt, E.-A. Kim, M. J. Lawler, D. Hai Lee, J. Davis, H. Eisaki, and S.-i. Uchida, J. Phys. Soc. Jpn. **81**, 011005 (2012).

[14] Y. Kohsaka, C. Taylor, K. Fujita, A. Schmidt, C. Lupien, T. Hanaguri, M. Azuma, M. Takano, H. Eisaki, H. Takagi, S. Uchida, and J. C. Davis, Science **315**, 1380 (2007).

[15] T. Hanaguri, C. Lupien, Y. Kohsaka, D.-H. Lee, M. Azuma, M. Takano, H. Takagi, and J. C. Davis, Nature (London) **430**, 1001 (2004).

[16] U. Chatterjee, J. Zhao, M. Iavarone, R. Di Capua, J. P. Castellan, G. Karapetrov, C. D. Malliakas, M. G. Kanatzidis, H. Claus, J. P. C. Ruff, F. Weber, J. van Wezel, J. C. Campuzano, R. Osborn, M. Randeria, N. Trivedi, M. R. Norman, and S. Rosenkranz, Nat. Commun. **6**, 6313 (2015).

[17] S. Blanco-Canosa, A. Frano, T. Loew, Y. Lu, J. Porras, G. Ghiringhelli, M. Minola, C. Mazzoli, L. Braicovich, E. Schierle, E. Weschke, M. Le Tacon, and B. Keimer, Phys. Rev. Lett. **110**, 187001 (2013).

[18] B. Hildebrand, T. Jaouen, C. Didiot, E. Razzoli, G. Monney, M.-L. Mottas, A. Ubaldini, H. Berger, C. Barreteau, H. Beck, D. R. Bowler, and P. Aebi, Phys. Rev. B **93**, 125140 (2016).

[19] J.-i. Okamoto, C. J. Arguello, E. P. Rosenthal, A. N. Pasupathy, and A. J. Millis, Phys. Rev. Lett. **114**, 026802 (2015).

[20] M. K. Kinyanjui, T. Björkman, T. Lehnert, J. Köster, A. Krasheninnikov, and U. Kaiser, Phys. Rev. B **99**, 024101 (2019).

[21] C. J. Arguello, S. P. Chockalingam, E. P. Rosenthal, L. Zhao, C. Gutiérrez, J. H. Kang, W. C. Chung, R. M. Fernandes, S. Jia, A. J. Millis, R. J. Cava, and A. N. Pasupathy, Phys. Rev. B **89**, 235115 (2014).

[22] I. Brihuega, O. Custance, R. Pérez, and J. M. Gómez-Rodríguez, Phys. Rev. Lett. **94**, 046101 (2005).

[23] A. V. Melechko, J. Braun, H. H. Weitering, and E. W. Plummer, Phys. Rev. B **61**, 2235 (2000).

[24] H. Shim, G. Lee, J.-M. Hyun, and H. Kim, New J. Phys. **17**, 093026 (2015).

[25] H. W. Yeom, D. M. Oh, S. Wippermann, and W. G. Schmidt, ACS Nano **10**, 810 (2016).

[26] D. E. Moncton, J. D. Axe, and F. J. DiSalvo, Phys. Rev. Lett. **34**, 734 (1975).

[27] D. E. Moncton, J. D. Axe, and F. J. DiSalvo, Phys. Rev. B **16**, 801 (1977).

[28] J. Dai, E. Calleja, J. Alldredge, X. Zhu, L. Li, W. Lu, Y. Sun, T. Wolf, H. Berger, and K. McElroy, Phys. Rev. B **89**, 165140 (2014).

[29] D. J. Eaglesham, S. McKernan, and J. W. Steeds, J. Phys. C **18**, L27 (1985).

[30] K. Ghoshray, B. Pahari, A. Ghoshray, V. V. Eremenko, V. A. Sirenko, and B. H. Suits, J. Phys. Condens. Matter **21**, 155701 (2009).

[31] A. Soumyanarayanan, M. M. Yee, Y. He, J. van Wezel, D. J. Rahn, K. Rossnagel, E. W. Hudson, M. R. Norman, and J. E. Hoffman, Proc. Natl. Acad. Sci. U.S.A. **110**, 1623 (2013).

[32] G. Gye, E. Oh, and H. W. Yeom, Phys. Rev. Lett. **122**, 016403 (2019).

[33] G. Kresse and J. Furthmüller, Phys. Rev. B **54,** 11169 (1996).

[34] P. E. Blöchl, Phys. Rev. B **50,** 17953 (1994).

[35] G. Kresse and D. Joubert, Phys. Rev. B **59,** 1758 (1999).

[36] J. P. Perdew, K. Burke, and M. Ernzerhof, Phys. Rev. Lett. **77,** 3865 (1996).

[37] S. Grimme, J. Comput. Chem. **27,** 1787 (2006).

[38] J. Tersoff and D. R. Hamann, Phys. Rev. Lett. **50,** 1998 (1983).

[39] A. Prodan, V. Marinkovi, R. Gril, N. Ramak, H. J. P. van Midden, F. W. Boswell, and J. C. Bennett, J. Vac. Sci. Technol. B **18,** 60 (2000).

[40] See Supplemental Material at http://link.aps.org/supplemental/10.1103/PhysRevLett.125.036804 for additional experimental data and DFT results.

[41] L. Nguyen, H.-P. Komsa, E. Khestanova, R. J. Kashtiban, J. J. P. Peters, S. Lawlor, A. M. Sanchez, J. Sloan, R. V. Gorbachev, I. V. Grigorieva, A. V. Krasheninnikov, and S. J. Haigh, ACS Nano **11,** 2894 (2017).

[42] B. Hildebrand, C. Didiot, A. M. Novello, G. Monney, A. Scarfato, A. Ubaldini, H. Berger, D. R. Bowler, C. Renner, and P. Aebi, Phys. Rev. Lett. **112,** 197001 (2014).

[43] P. B. Littlewood and T. M. Rice, Phys. Rev. Lett. **48,** 27 (1982).